

# Through-Thickness Variations of Deformed and Annealed Microstructures in ECAE-Processed Copper

O.V. MISHIN and J.R. BOWEN

Through-thickness variations of the microstructure in copper processed using equal channel angular extrusion (ECAE) to a strain of  $\sim 10$  without rotations between passes have been investigated in deformed and partially recrystallized conditions. It is found that the through-thickness heterogeneity in the deformed sample follows the distribution of strain imposed by ECAE, where lower strain is imparted to the material that passes through the outer die corner. Also, the macroscopic distribution of recrystallized grains as a function of depth in the billet is found to be in correspondence to the applied strain. Compared to other inspected layers the bottom part of the billet was less refined after ECAE and remained less recrystallized after annealing.

DOI: 10.1007/s11661-009-9852-y

© The Minerals, Metals & Materials Society and ASM International 2009

## I. INTRODUCTION

EQUAL channel angular extrusion (ECAE)<sup>[1,2]</sup> is a deformation technique that has attracted much attention due to its capability to achieve large strains in bulk samples through multiple passes without significantly changing the dimensions of the extruded billet. Despite significant interest and numerous publications describing microstructures produced by this technique, through-thickness variations of microstructural parameters after multiple-pass ECAE have been analyzed to a lesser extent, because most previous characterizations have been performed near the centerline of the billet. Such variations can be expected considering a heterogeneous strain distribution imposed by this deformation process.<sup>[3–8]</sup> The strain heterogeneity was found to strongly affect texture in different layers of ECAE-processed samples.<sup>[4–6]</sup> A similar situation during rolling, *i.e.*, a strongly heterogeneous strain distribution producing substantially different textures,<sup>[9–11]</sup> has been shown to result in pronounced through-thickness variations of the rolled microstructure.<sup>[9,11]</sup> Considerable through-thickness variations of the microstructure are likely to be produced also by the ECAE process. Indeed, Li *et al.*,<sup>[5,6]</sup> investigating the microstructure in copper after one ECAE pass, found banded structures in the center and in the top part of the billet, while the shape of grains in the bottom part was very similar to that in the billet before ECAE.<sup>[6]</sup> After rotating the billet 180 deg about its longitudinal axis, the morphology

of deformed grains changed, but the microstructure and texture remained strongly heterogeneous through the thickness.<sup>[6]</sup> Having studied the variation of the microstructure in aluminum ECAE deformed with 90 deg rotations (route Bc), Terhune *et al.*<sup>[12]</sup> suggested that through-thickness heterogeneities were present after a small number of passes, but after many passes, the deformation texture and the microstructure were reported to become homogeneous. It should be noted that Terhune *et al.*<sup>[12]</sup> investigated only the top half of the billet thickness using relatively small EBSD maps for microstructural characterization. Different conclusions have been drawn by Necker *et al.*,<sup>[13]</sup> who, after inspecting the microstructure in copper annealed after ECAE, suggested that multiple passes using route Bc did not homogenize strain in deformed samples. It is known that route Bc produces substantial local variations in the microstructure,<sup>[14,15]</sup> which can bias the analysis of through-thickness variations. Although ECAE without rotations (route A) also produces heterogeneous microstructures in copper, local heterogeneities along the centerline have been observed to be less severe compared to those after route Bc.<sup>[15]</sup> To date, no systematic experimental study of through-thickness variations of microstructural parameters after multiple-pass route A ECAE has been presented. The possible effects of such variations on recrystallization in route A samples also require detailed analysis. When studying recrystallization, it is important to identify areas where recrystallized grains tend to emerge. In a previous study on ECAE-processed copper, where partially recrystallized microstructures were observed after long-term room-temperature storage, such areas were characterized as high misorientation regions.<sup>[15]</sup> By using the same characterization approach for the deformed and partially recrystallized samples, it should be possible to analyze quantitatively which regions are consumed most during recrystallization and correspondingly which regions evolve the least. Therefore, both macroscopic through-thickness variations and

O.V. MISHIN, Senior Scientist, is with the Center for Fundamental Research: Metal Structures in Four Dimensions, Materials Research Division, Risø National Laboratory for Sustainable Energy, Technical University of Denmark, DK-4000 Roskilde, Denmark. Contact e-mail: olmishin@lycos.com J.R. BOWEN, Senior Scientist, is with the Fuel Cells and Solid State Chemistry Division, Risø National Laboratory for Sustainable Energy, Technical University of Denmark. Manuscript submitted October 2, 2008.

Article published online June 6, 2009

microscopic local heterogeneities are characterized in the present study.

In this work, microstructures in three different layers are analyzed in copper, heavily ECAE deformed without billet rotations. In each layer, regions of well-refined and less-refined microstructure are identified and the progress of recrystallization in these layers is followed after controlled annealing. Since a comparative study of microstructures in different layers requires significant statistics characterizing large sample areas, the electron backscatter diffraction (EBSD) technique is extensively used in this experiment for quantitative analysis of microstructural parameters.

## II. EXPERIMENTAL

Annealed oxygen-free high conductivity (OFHC) copper samples (99.98 pct purity) were machined into 15-mm-diameter billets of length 100 mm. Deformation was performed at room temperature in a 120-deg sharp cornered die<sup>[3]</sup> without billet rotation between passes. The die yields 0.67 von Mises equivalent strain per deformation pass. For the present work, the microstructure has been investigated after 15 passes or a von Mises strain of 10. Billets were lubricated by dipping in a colloidal graphite suspension followed by drying; typically 3 to 4 coatings were applied between deformation passes. The extruded billets and samples were kept at approximately  $-20\text{ }^{\circ}\text{C}$  for long-term storage between essential sample preparation and characterization operations. This is vital for preserving the as-deformed structure, because partial recrystallization can occur during room-temperature storage of ECAE processed copper.<sup>[15]</sup>

A part of the deformed sample was also annealed at  $160\text{ }^{\circ}\text{C}$  for 2 hours. A preliminary investigation<sup>[16]</sup> showed that after this heat treatment the original hardness decreased by  $\sim 13$  pct, which suggested that deformation structures still occupied a significant volume fraction in this partially recrystallized material.

Samples of the initial, deformed, and annealed materials were sectioned along the symmetry plane of the billet to produce specimens that contained the billet axis and the vertical direction, also referred to as the extrusion and normal directions (ED-ND, Figure 1). Microstructural characterization of these specimens was performed using EBSD in a Zeiss Supra-35 field-emission gun scanning electron microscope equipped with the Oxford Instruments-HKL Channel 5 system and Nordlys detector. The initial undeformed material was characterized in the center and at 1 mm below the surface of the billet using a step size of  $4\text{ }\mu\text{m}$ . For the deformed sample, three different depths were probed: 1 mm from the top surface (the surface that passed through the inner corner of the ECAE die), along the centerline and at 0.4 mm from the bottom surface. These depths correspond to 6.7, 50, and 97.3 pct from the top surface, which are hereafter referred to as the



Fig. 1—A sectioned billet and the coordinate system.

top, center, and bottom of the billet, respectively. For each depth of the deformed sample, several orientation maps were produced with a step size of  $70\text{ nm}$  each covering approximately  $3400\text{ }\mu\text{m}^2$ . In addition, fine step-size ( $30\text{ nm}$ ) maps covering smaller areas were collected to investigate the deformed microstructure in more detail. Larger step sizes,  $0.5$  to  $0.7\text{ }\mu\text{m}$ , were used for sampling crystallographic texture in the center layer of the extruded billet. At least two  $3400\text{-}\mu\text{m}^2$  maps with a step size of  $100\text{ nm}$  were produced from each depth of the annealed sample. Because of the presence of orientation noise in the EBSD data, the boundary statistics in this work included only misorientations  $>2\text{ deg}$ .

Following previous work,<sup>[15]</sup> the deformed microstructure was divided into regions containing predominantly high-angle misorientations (high-misorientation regions (HMRs)) and regions containing predominantly low-angle misorientations (low misorientation regions (LMRs)). The LMRs were classified as regions  $>2.5\text{ }\mu\text{m}^2$  defined by misorientations below  $5\text{ deg}$ . Thus, each LMR represents a sufficiently large area in which the microstructure contains predominantly very low misorientations. The remaining area in the microstructure was defined as consisting of HMRs. Recrystallized areas after annealing were identified using the following routine. At first, a grain reconstruction process was carried out using a boundary definition of  $10\text{ deg}$ . Then, a subset of recrystallized regions was created automatically. The subset included the reconstructed grains with an average internal misorientation of less than  $1.5\text{ deg}$  and with an area greater than  $0.5\text{ }\mu\text{m}^2$ . A small number of grains missed using the automated procedure were added manually to the recrystallized area subset. Such manually added grains were detected based on several features. These included the size of the recrystallized grains (being larger than the size of cells and subgrains in the deformed matrix), the higher EBSD pattern quality, and the fact that the recrystallized grains are not subdivided by low-angle boundaries (LABs). Additionally, in many cases, recrystallized grains could be identified by the presence of twin boundaries. Based on the results of a previous investigation,<sup>[17]</sup> only boundaries with deviations  $<3\text{ deg}$  from the ideal twin misorientation were classified as twin boundaries.

### III. RESULTS

#### A. Initial Microstructure

An optical micrograph illustrating the initial microstructure in the center of the undeformed billet is shown in Figure 2. The microstructure is fully recrystallized and is characterized by a high density of annealing twins. The mean grain size in this sample was estimated to be 40 to 45  $\mu\text{m}$ . The microstructure in the subsurface regions was more homogeneous than in the center of the billet, where a larger fraction of coarse ( $>100 \mu\text{m}$ ) crystallites was found (Table I). Note that no distinction between the top and bottom subsurface layers is made in Table I, because the microstructure of these layers before deformation was very similar. In each layer, a weak texture representing the cube and rolling texture components was observed.

#### B. Deformed Microstructure

A fine step-size EBSD map from the center of the deformed billet is presented in Figure 3. It is seen that the microstructure is composed of extended structures slightly deviated from the extrusion direction. The extended structures are subdivided by LABs. A number of small (0.2 to 0.4  $\mu\text{m}$ ) elongated subgrains fully surrounded by high-angle boundaries (HABs) are also present in the microstructure. The average spacings between boundaries  $>2$  deg along the ND and ED were 0.2 and 0.3  $\mu\text{m}$ , respectively. Similar boundary spacings were found in the two other layers.

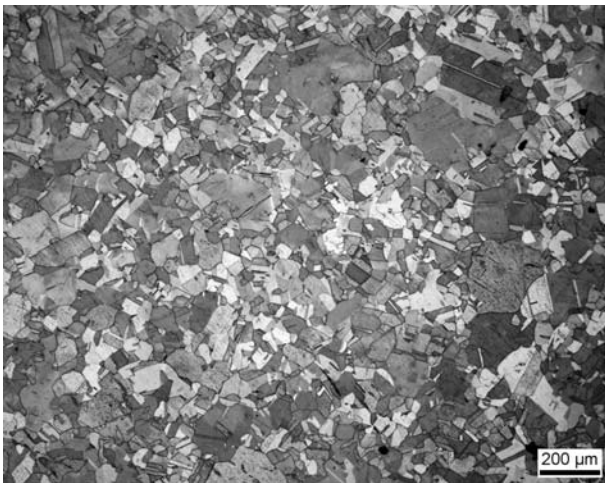


Fig. 2—Optical micrograph illustrating the microstructure of the initial material in the center of the billet.

Larger EBSD maps for the top, center, and bottom layers of the deformed sample are given in Figure 4. All the maps show extended structures typically aligned at 5 to 11 deg to the extrusion direction (for a von Mises strain of 10, the theoretical angle of an element deformed by simple shear is  $\sim 7$  deg). These structures are intersected by boundaries at 50 to 60 deg relative to the ED that is close to the orientation of the theoretical shear plane for the 120-deg die. Microstructures at the three different depths appear morphologically similar. However, they demonstrate somewhat different HAB spacings and a different degree of uniformity.

The microstructure of the top layer appears very uniform and is subdivided predominantly by elongated subgrains (Figure 4(a)). Extended regions with similar orientations (with low boundary misorientations) are also present, but they are narrow, typically  $<1 \mu\text{m}$  in width. The area fraction of such low misorientation regions was only 13 pct in this layer (Table II). The spacing between HABs is small and the fraction of HABs in the EBSD maps is 57 pct (Table II). A similar HAB fraction was obtained in the maps recorded along the centerline; however, here, broad (2 to 4  $\mu\text{m}$ ) bands of similar orientations containing LABs were occasionally observed along with fine subgrains separated by HABs (Figure 4(b)). Therefore, the fraction of the LMRs here was greater than in the top layer (Table II). Crystallographic orientations of the LMRs and HMRs from the center region shown in the Figure 4(b) are presented in Figure 5. It is seen that the orientations of the HMRs compose a weak texture that can be

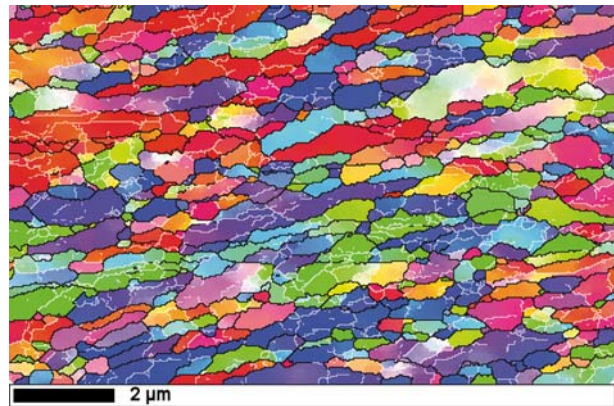


Fig. 3—Fine step-size EBSD map for a small region in the center of the deformed billet. Black lines depict HABs ( $>15$  deg). Misorientations 2 to 15 deg are shown as white lines. The extrusion direction is horizontal.

Table I. Microstructural Parameters for the Undeformed Billet

Layer	Average HAB Spacing Excluding Twins ( $\mu\text{m}$ )	Average HAB Spacing Including Twins ( $\mu\text{m}$ )	Fraction of Twin Boundaries (Pct)	Area Fraction of Grains $>100 \mu\text{m}$ Including Twins (Pct)
	ND/ED	ND/ED		
Subsurface	39/40	22/22	33	8
Center	44/43	23/22	36	17

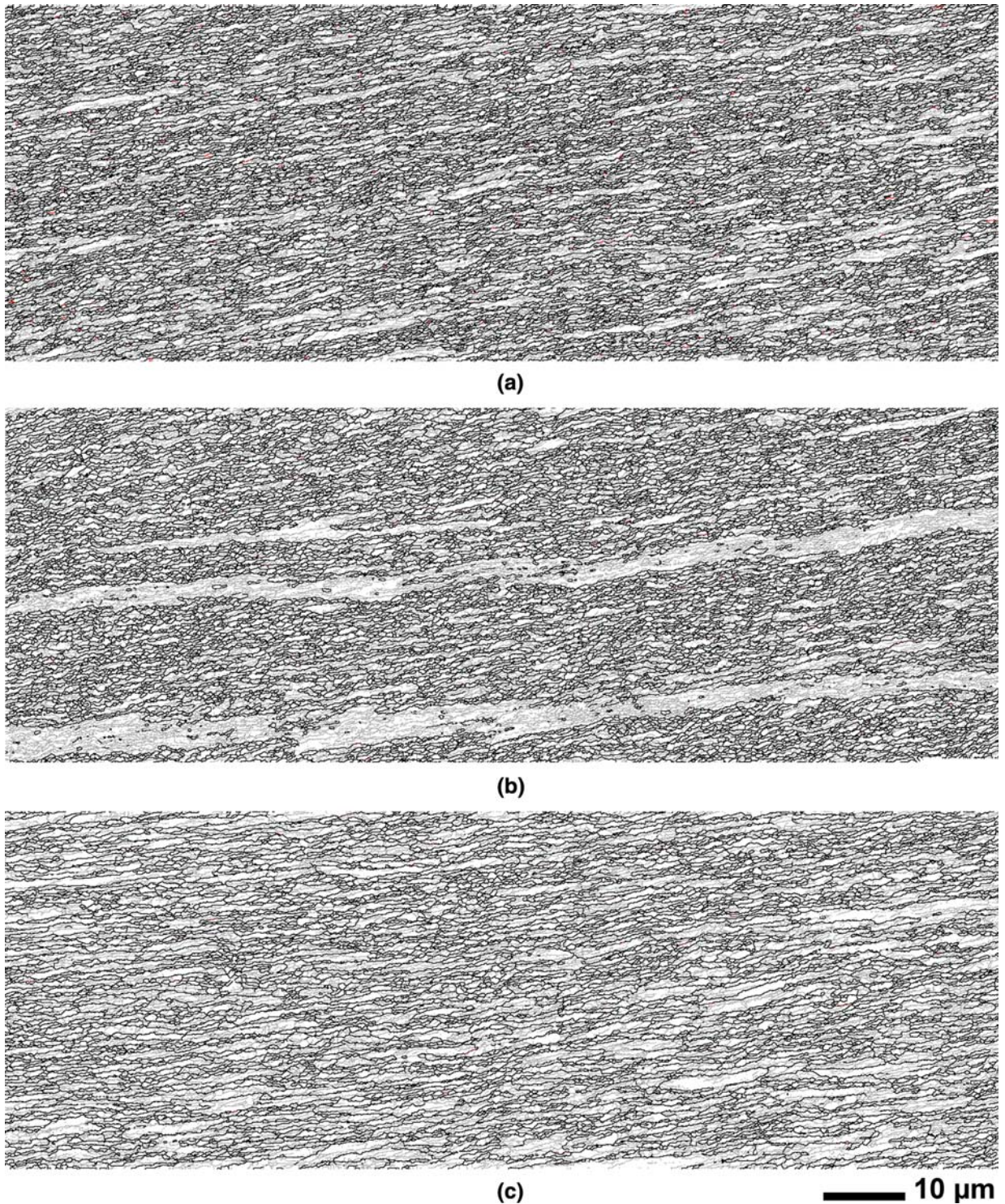


Fig. 4—EBSD misorientation maps for the deformed sample: (a) top, (b) center, and (c) bottom. HABs (>15 deg) are shown in black except for the twin boundaries shown in red. Misorientations 2 to 15 deg are shown as thin gray lines. The extrusion direction is parallel to the scale bar.

identified as shear-type texture (Figure 5(a)). The LMR texture in this region is dominated by orientations of two broad bands that belong to a single texture component. This results in a very high maximum intensity in the LMR pole figure (Figure 5(b)). A second component is also distinguished in Figure 5(b);

however, it is very weak. Both components can be described as  $B_{\theta}/\bar{B}_{\theta}$  components of the ECAE texture,<sup>[18]</sup> although the peaks in the pole figure are slightly shifted from the exact positions of the ideal  $B_{\theta}/\bar{B}_{\theta}$  orientations (compare with Figure 5(d) in Reference 18). In the given sample, every broad LMR band inspected in the center

**Table II. Microstructural Parameters for the Deformed and Partially Recrystallized Billets**

Layer	Deformed Billet				Partially Recrystallized Billet		
	Average HAB Spacing ( $\mu\text{m}$ ) ND/ED	HAB Fraction (Pct)	Area Fraction (Pct)		Area Fraction (Pct)		
			HMRs	LMRs	HMRs	LMRs	Recrystallized
Top	0.34/0.62	57	87	13	61	10	29
Center	0.36/0.60	58	81	19	52	19	29
Bottom	0.43/0.78	51	72	28	63	28	9

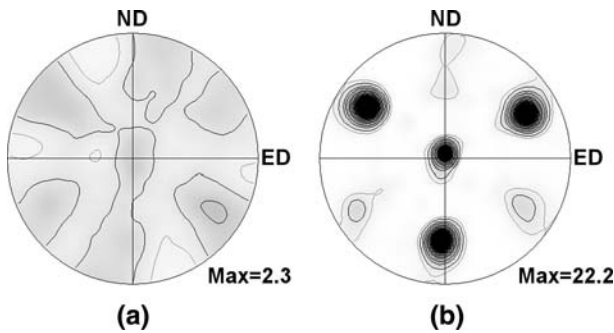


Fig. 5—{111} pole figures showing crystallographic orientations of (a) HMRs and (b) LMRs in the EBSD map presented in Fig. 4(b) (covering an area of  $\sim 3400 \mu\text{m}^2$ ; also Fig. 8(a)). Contour lines: 0.5, 1, 2, 3, 5, 10, 15, and 20.

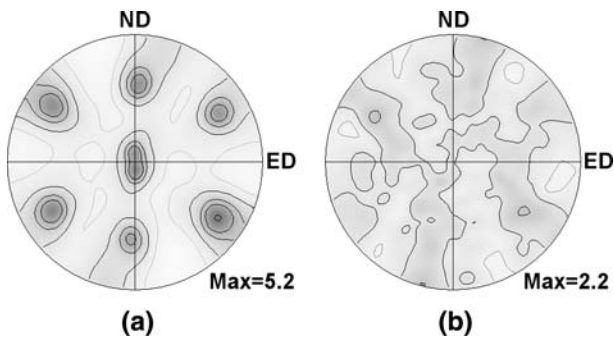


Fig. 6—{111} pole figures showing orientations combined from several regions in the center of the billet: (a) from a total area of  $460,000 \mu\text{m}^2$  in the deformed sample and (b) orientations of recrystallized grains after annealing at  $160 \text{ }^\circ\text{C}$  for 2 h. Contour lines: 0.5, 1, 2, 3, and 5.

was found to have orientations close to either of these components. Both components appear in similar intensities in the pole figure representing texture data from a large sample area (Figure 6(a)).

The largest frequency of the LMRs, 28 pct, was found close to the bottom surface (Figure 4(c)). Also, the average HAB spacing here becomes larger than in the other layers (Table II). Consequently, the fraction of HABs in this layer was lower than in the other two layers, 51 pct.

### C. Partially Recrystallized Microstructure

The microstructure of the partially recrystallized sample is shown in Figure 7. It is immediately apparent

that the number of recrystallized grains, *i.e.*, grains free of dislocation boundaries, is much smaller in the bottom layer than in the other two layers, where the fraction recrystallized approached 30 pct (Table II). The recrystallized grains were typically less than  $10 \mu\text{m}$  and frequently contained annealing twins. Most of the recrystallized grains appear to originate in highly refined HMRs (Figure 8(b)). The growing grains are typically surrounded by HABs; however, in some locations, low misorientations between the recrystallized grains and nonrecrystallized areas were also observed. Analysis of crystallographic orientations of the recrystallized grains shows that many of these grains have orientations present in the deformed sample. However, the recrystallization texture is weaker and more scattered than the texture of the extruded material (Figure 6(b)).

## IV. DISCUSSION

### A. Deformation Structures

The results obtained in the present experiment demonstrate that a uniform ultra-fine-grain structure is not achieved in OFHC copper during route A ECAE even after a strain of  $\sim 10$ . The microstructure resembles “ribbon grains” observed in aluminum,<sup>[19]</sup> but with much smaller boundary spacing and a smaller fraction of HABs.<sup>[20]</sup> However, the fraction of HABs is significant, approaching 60 pct in a large portion of the billet, but reduces to  $\sim 50$  pct near the volumes that have passed through the outer die corner. Furthermore, the spacing between HABs is not homogeneous through the thickness, giving greater values near the bottom. Obviously, this type of heterogeneity is due to the nonuniform strain distribution through the billet thickness.<sup>[3–8]</sup> For the same die and similar friction conditions, it was established that the applied strain was much lower in the bottom of the billet than in its center and the top, where the applied strain was relatively uniform.<sup>[3]</sup> Therefore, the greater HAB spacings and lower fractions of HABs in the bottom reflect the lower strain in this part of the ECAE-deformed billet.

In addition to the through-thickness variations, there are significant local heterogeneities in the microstructure, especially near the centerline, where broad and extended bands with the predominance of LABs were found along with well-refined regions (Figure 4(b)). It is suggested that the broad bands originate from the coarse grains that were frequent in the initial microstructure in the middle of the billet (Figure 2 and Table I). Apparently, some of

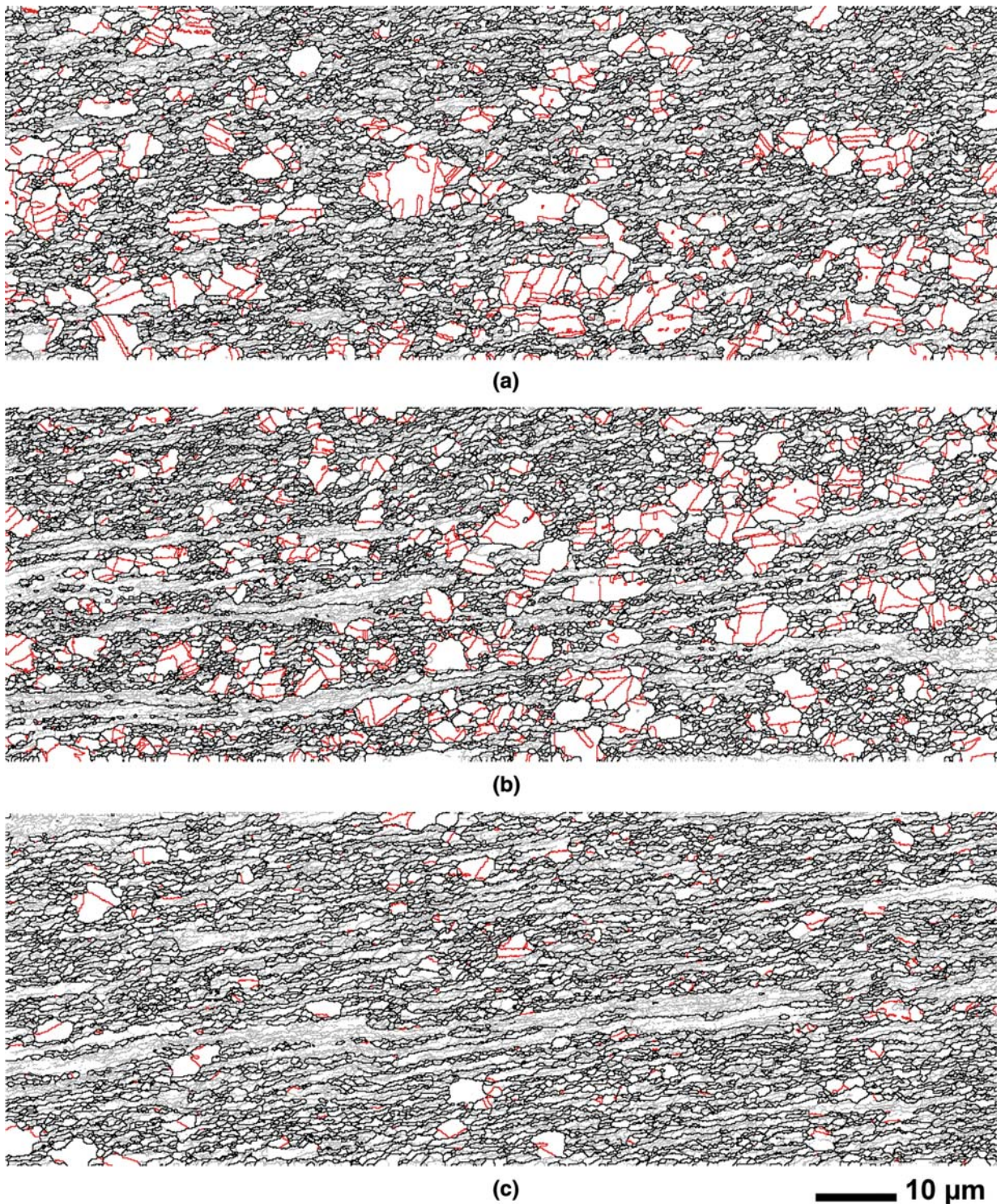


Fig. 7—EBSD misorientation maps for the partially recrystallized sample: (a) top, (b) center, and (c) bottom. The HABs ( $>15$  deg) are shown in black, and twin boundaries are shown in red. Thin gray lines correspond to 2 to 15 deg misorientations. The extrusion direction is parallel to the scale bar.

these grains were able to resist breaking into highly misoriented volumes even after such a high ECAE strain. The broad bands constitute the major fraction of the LMRs in the billet body and have orientations close to the ideal  $B_\theta/\bar{B}_\theta$  components that are considered to belong to

the main ideal orientations of the ECAE texture.<sup>[18,21]</sup> The  $B_\theta/\bar{B}_\theta$  components have previously been observed to strengthen in copper and aluminum billets during multi-pass route A ECAE through a 90-deg die.<sup>[21,22]</sup> According to Li *et al.*,<sup>[21]</sup> the development of these components in

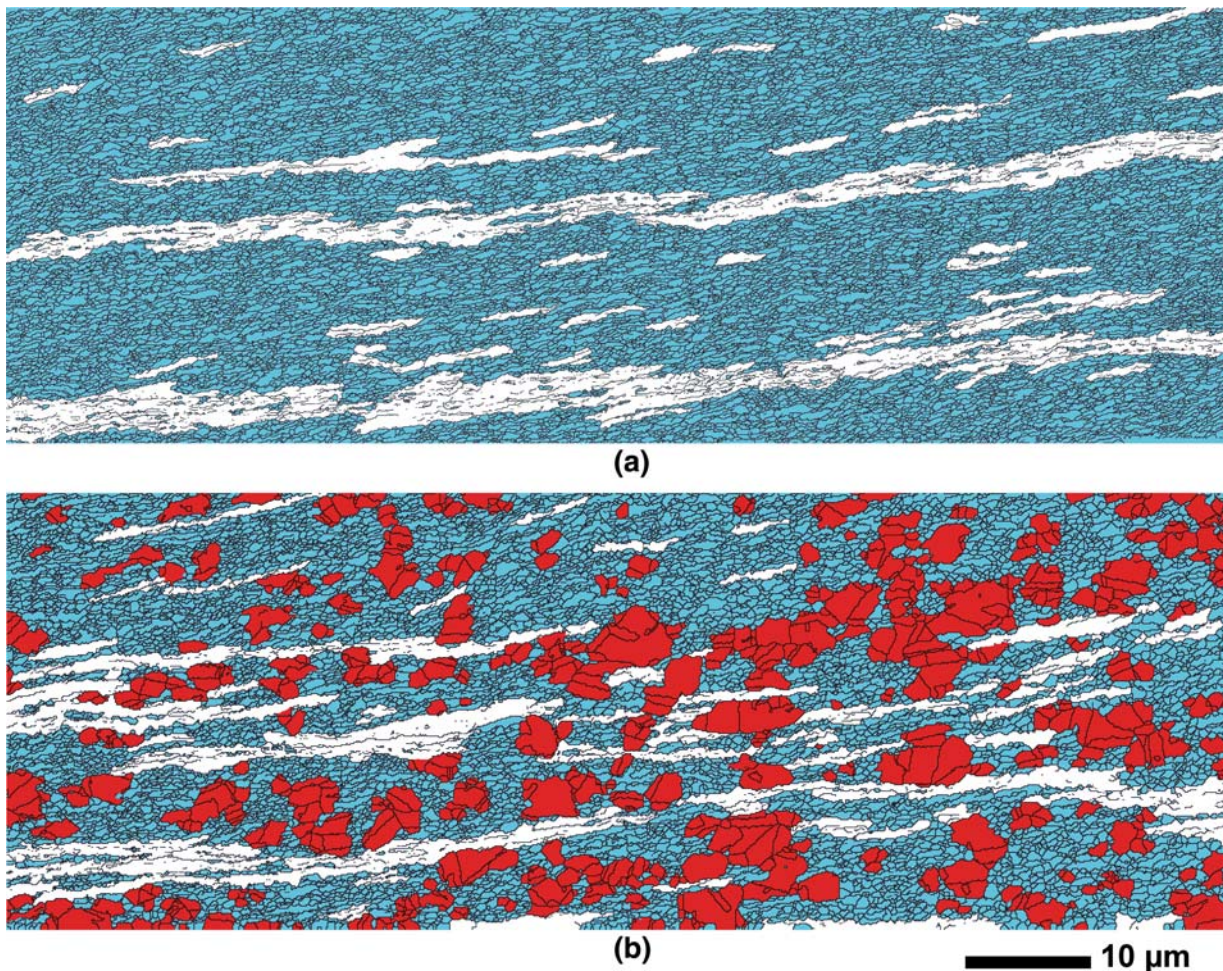


Fig. 8—EBSD maps showing regions in the center of deformed and partially recrystallized samples: (a) deformed sample and (b) partially recrystallized sample. The maps demonstrate the microstructure divided into high misorientation (blue), low misorientation (white), and recrystallized (red) regions, with misorientations of  $>5$  deg shown in black. The extrusion direction is parallel to the scale bar.

material extruded through a 90-deg ECAE die is predicted by the Taylor model. However, we are not aware of any modeling data that would predict strengthening of the same components also for materials heavily strained in a 120-deg die. In our experiment, we find these components to be distributed very heterogeneously in the microstructure; they clearly dominate within the LMRs, while in the HMRs, their intensities are much weaker.

In contrast to the route A sample characterized in a previous study,<sup>[15]</sup> where extended bands closely aligned to the ED were disrupted by colonies of shear bands, many LMRs in the present sample are significantly extended without substantial disruption. In general, the magnitude of shear banding in this sample was less than in the sample extruded using a different die.<sup>[15]</sup> As expected, due to the larger strain applied in the present experiment, the boundary spacing as well as the LAB fraction and the total fraction of LMRs are smaller than those found in the route A sample deformed to a strain of 8.<sup>[15]</sup> The LMR/HMR fractions appear to be more sensitive parameters than the fractions of HABs/LABs or the boundary spacing. For example, whereas the latter parameters are very

similar for the top and the center of the billet (Table II), the LMR/HMR fractions vary considerably between these layers, better reflecting the heterogeneity of the microstructure.

Another aspect that is important to emphasize, considering the ongoing discussion on whether recrystallized grains occasionally observed in some non-heat-treated ECAE samples are produced by either dynamic or static recrystallization,<sup>[23–26]</sup> is that no recrystallized grains were observed in the given material directly after ECAE. Also, no recrystallized grains appeared after 1 year of cold storage. This result provides strong evidence and supports the previous suggestion<sup>[15]</sup> that, if recrystallized grains develop in ECAE-processed copper stored at room temperature, they are most likely the result of postdeformation static recrystallization.

### B. Effect of Annealing

During annealing, the ECAE-deformed microstructure recovers and some of the subgrains start growing. It is of course of interest to know where exactly the original nuclei appeared and what orientation

relationships they had with the deformed microstructure during nucleation, but in postmortem observations, the evidence is frequently lost as the grains grow, encounter different cells and subgrains, and change their boundary misorientations. This is especially true for materials prone to multiple twinning such as copper, where growing grains quickly develop annealing twins, which produces new orientations that were not present in the deformed material. Still both close to the top surface and in the center, and especially in the poorly recrystallized bottom part, there are recrystallized grains that could partially preserve their orientation relationship with the deformed matrix. Low-angle misorientations between the growing grains and the matrix were found in a number of locations (Figure 7). Therefore, a significant fraction of the recrystallized grains will contain orientations observed in the deformed sample, which is confirmed by the data in Figure 6(b). Multiple twinning results in the recrystallization texture being more scattered than the texture of the deformed sample, but in general the recrystallization texture is similar to that in the HMRs (compare Figures 6(b) and 5(a)). The  $\Sigma 3$  boundaries appear to be the only boundary type to have clearly increased frequencies in the distribution of the coincident site lattice (CSL) misorientations (Figure 9).

Similar to the observations made in ECAE-processed copper partially recrystallized during long-term room-temperature storage,<sup>[15]</sup> the grains recrystallized during controlled annealing were most frequently found inside the HMRs. Nucleation inside the HMRs is not surprising, because for the same effective strain, the driving force for recrystallization and the boundary mobility should be greater in these regions than in the LMRs. In the present study, we not only identify regions where recrystallized grains are typically observed, but we can also quantify the relative loss of the HMRs and LMRs by comparing their area fractions in the deformed and partially recrystallized conditions. Considering Table II, it is seen that the relative loss of the HMRs during recrystallization is significant compared to that of the LMRs: the initial fraction of the LMRs remains virtually unchanged in the partially recrystallized

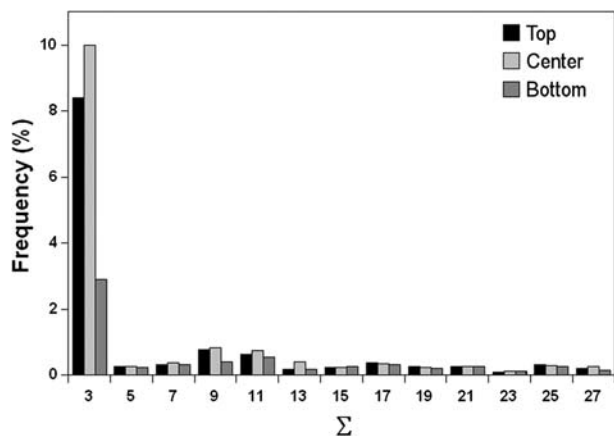


Fig. 9—Distribution of low CSL boundaries ( $3 \leq \Sigma \leq 27$ ) for the partially recrystallized sample. Here  $\Sigma$  boundaries are defined using the standard Brandon criterion.

condition, while recrystallization consumes a significant fraction of the HMRs.

Comparing the progress of recrystallization in the three different layers, it is evident that it generally follows the distribution of strain. The bottom part that is known to be strained less than the other two layers revealed larger HAB spacings, the lowest fraction of HABs and HMRs, and it remained largely nonrecrystallized. In the other two layers of the billet, where the differences in the effective strain during deformation were small, and where the HAB fractions were similar (Table II), the loss of the HMRs results in similar recrystallized fractions.

## V. CONCLUSIONS

The through-thickness heterogeneity of microstructure and its subsequent effects upon partial recrystallization have been characterized in OFHC copper deformed by route A ECAE to a von Mises strain of 10. From the present work, the following is concluded.

1. Significant through-thickness heterogeneity of the deformed microstructure in terms of HAB fraction, HAB spacing, and the distribution of low and high misorientation regions was observed in the sample. Interpreting the microstructure in terms of LMR/HMR statistics provides an improved description of microstructural heterogeneity compared to the average boundary spacing and fraction of HABs alone.
2. The through-thickness heterogeneity generally follows the distribution of strain imposed by ECAE. Near the bottom of the billet, where lower strain is imparted to the material that passes through the outer die corner, the fractions of HABs and HMRs are considerably smaller than in the top part and in the center, where the applied strain was higher.
3. No evidence of dynamic recrystallization was found in the billet studied in this work. No recrystallized grains were observed directly after ECAE and after 1 year of storage at  $-20^\circ\text{C}$ . Annealing at  $160^\circ\text{C}$  for 2 hours produced partial recrystallization of the deformed microstructure.
4. The macroscopic distribution of recrystallized grains as a function of depth in the billet was observed to be heterogeneous and in correspondence to the applied strain. The bottom part of the billet that is known to be strained less than other layers remained less recrystallized. Locally, recrystallization was also found to be heterogeneous, where recrystallized grains were typically observed in HMRs. In the partially recrystallized condition, the initial fraction of the LMRs remained virtually unchanged for all the positions inspected across the thickness.

## ACKNOWLEDGMENTS

Financial support from the Danish National Research Foundation *via* the Center for Fundamental



Research: Metal Structures in Four Dimensions is acknowledged. The authors are grateful to Drs. D. Juul Jensen, N. Hansen, S. van Boxel, and Professor A. Godfrey for useful discussions of the results. We thank Professor P.B. Prangnell, Manchester Materials Science Centre, for access to ECAE facilities, and S. Martin for aid in the processing of material.

## REFERENCES

1. V.M. Segal, V.I. Reznikov, A.E. Drobyshevskiy, and V.I. Kopylov: *Russ. Metall.*, 1981, vol. 1, pp. 99–105.
2. V.M. Segal: *Mater. Sci. Eng. A*, 1995, vol. 197, pp. 157–64.
3. J.R. Bowen, A. Gholinia, S.M. Roberts, and P.B. Prangnell: *Mater. Sci. Eng. A*, 2000, vol. 287, pp. 87–99.
4. S. Li, M.A.M. Bourke, I.J. Beyerlein, D.J. Alexander, and B. Clausen: *Mater. Sci. Eng. A*, 2004, vol. 382, pp. 217–36.
5. S. Li, I.J. Beyerlein, C.T. Necker, D.J. Alexander, and M. Bourke: *Acta Mater.*, 2004, vol. 52, pp. 4859–75.
6. S. Li, I.J. Beyerlein, and C.T. Necker: *Acta Mater.*, 2006, vol. 54, pp. 1397–408.
7. S.J. Oh and S.B. Kang: *Mater. Sci. Eng. A*, 2003, vol. 343, pp. 107–15.
8. L.S. Tóth, R. Arruffat Massion, L. Germain, S.C. Baik, and S. Suwas: *Acta Mater.*, 2004, vol. 52, pp. 1885–98.
9. B. Major: *Mater. Sci. Technol.*, 1992, vol. 8, pp. 510–15.
10. O.V. Mishin, E.M. Lauridsen, N.C. Krieger Lassen, G. Brückner, T. Tschentscher, B. Bay, D. Juul Jensen, and H.F. Poulsen: *J. Appl. Cryst.*, 2000, vol. 33, pp. 364–71.
11. O.V. Mishin, B. Bay, G. Winther, and D. Juul Jensen: *Acta Mater.*, 2004, vol. 52, pp. 5761–70.
12. S.D. Terhune, D.L. Swisher, K. Oh-Ishi, Z. Horita, T.G. Langdon, and T.R. McNelley: *Metall. Mater. Trans. A*, 2002, vol. 33A, pp. 2173–84.
13. C.T. Necker, D.J. Alexander, and I.J. Beyerlein: *Mater. Sci. Forum*, 2005, vols. 495–497, pp. 857–64.
14. A. Gholinia, P.B. Prangnell, and M.V. Markushev: *Acta Mater.*, 2000, vol. 48, pp. 1115–30.
15. O.V. Mishin and A. Godfrey: *Metall. Mater. Trans. A*, 2008, vol. 39A, pp. 2923–30.
16. S. Martin: Risø National Laboratory for Sustainable Energy, Roskilde, unpublished research, 2007.
17. O.V. Mishin and X. Huang: *Mater. Sci. Forum*, 1999, vols. 294–296, pp. 401–04.
18. S. Li, I.J. Beyerlein, and M.A.M. Bourke: *Mater. Sci. Eng. A*, 2005, vol. 394, pp. 66–77.
19. P.B. Prangnell, J.R. Bowen, and P.J. Apps: *Mater. Sci. Eng. A*, 2004, vols. 375–377, pp. 178–85.
20. O.V. Mishin, D. Juul Jensen, and N. Hansen: *Mater. Sci. Eng. A*, 2003, vol. 342, pp. 320–28.
21. S. Li, I.J. Beyerlein, and D.J. Alexander: *Mater. Sci. Eng. A*, 2006, vol. 431, pp. 339–45.
22. J.C. Werenskiold and H.J. Roven: *Mater. Sci. Eng. A*, 2005, vols. 410–411, pp. 174–77.
23. Y. Estrin, N.V. Isaev, S.V. Lubenets, S.V. Malykhin, A.T. Pugachov, V.V. Pustovalov, E.N. Reshetnyak, V.S. Fomenko, L.S. Fomenko, S.E. Shumilin, M. Janeczek, and R.J. Hellmig: *Acta Mater.*, 2006, vol. 54, pp. 5581–90.
24. A.L. Etter, T. Baudin, C. Rey, and R. Penelle: *Mater. Characterization*, 2006, vol. 56, pp. 19–25.
25. F.H. Dalla Torre, A.A. Gazder, C.F. Gu, C.H.J. Davies, and E.V. Pereloma: *Metall. Mater. Trans. A*, 2007, vol. 38A, pp. 1080–95.
26. F.H. Dalla Torre, A.A. Gazder, E.V. Pereloma, and C.H.J. Davies: *J. Mater. Sci.*, 2007, vol. 42, pp. 9097–11.